



Improved Measurement of the Partial-Rate CP Asymmetry in $B^+ \rightarrow K^0\pi^+$ and $B^- \rightarrow \bar{K}^0\pi^-$ Decays

Y. Unno,³ K. Suzuki,⁹ K. Abe,⁹ K. Abe,⁴⁴ T. Abe,⁴⁵ I. Adachi,⁹ H. Aihara,⁴⁶ M. Akatsu,²³ Y. Asano,⁵¹
T. Aso,⁵⁰ V. Aulchenko,² T. Aushev,¹³ S. Bahinipati,⁵ A. M. Bakich,⁴¹ Y. Ban,³⁴ S. Banerjee,⁴² A. Bay,¹⁹
I. Bedny,² P. K. Behera,⁵² I. Bizjak,¹⁴ A. Bondar,² A. Bozek,²⁸ M. Bračko,^{21,14} J. Brodzicka,²⁸ T. E. Browder,⁸
B. C. K. Casey,⁸ P. Chang,²⁷ Y. Chao,²⁷ K.-F. Chen,²⁷ B. G. Cheon,⁴⁰ R. Chistov,¹³ S.-K. Choi,⁷ Y. Choi,⁴⁰
Y. K. Choi,⁴⁰ M. Danilov,¹³ L. Y. Dong,¹¹ J. Dragic,²² A. Drutskoy,¹³ S. Eidelman,² V. Eiges,¹³ Y. Enari,²³
F. Fang,⁸ N. Gabyshev,⁹ A. Garmash,^{2,9} T. Gershon,⁹ B. Golob,^{20,14} R. Guo,²⁵ J. Haba,⁹ F. Handa,⁴⁵
H. Hayashii,²⁴ M. Hazumi,⁹ L. Hinze,¹⁹ T. Hokuue,²³ Y. Hoshi,⁴⁴ W.-S. Hou,²⁷ H.-C. Huang,²⁷ T. Iijima,²³
K. Inami,²³ A. Ishikawa,²³ R. Itoh,⁹ H. Iwasaki,⁹ Y. Iwasaki,⁹ H. K. Jang,³⁹ J. H. Kang,⁵⁵ J. S. Kang,¹⁶
P. Kapusta,²⁸ S. U. Kataoka,²⁴ N. Katayama,⁹ H. Kawai,³ H. Kawai,⁴⁶ N. Kawamura,¹ T. Kawasaki,³⁰ H. Kichimi,⁹
D. W. Kim,⁴⁰ H. J. Kim,⁵⁵ Hyunwoo Kim,¹⁶ J. H. Kim,⁴⁰ S. K. Kim,³⁹ K. Kinoshita,⁵ S. Kobayashi,³⁷
S. Korpar,^{21,14} P. Krizan,^{20,14} P. Krokovny,² R. Kulasiri,⁵ S. Kumar,³³ A. Kuzmin,² Y.-J. Kwon,⁵⁵ J. S. Lange,^{6,36}
G. Leder,¹² S. H. Lee,³⁹ J. Li,³⁸ A. Limosani,²² S.-W. Lin,²⁷ D. Liventsev,¹³ J. MacNaughton,¹² F. Mandl,¹²
D. Marlow,³⁵ H. Matsumoto,³⁰ T. Matsumoto,⁴⁸ A. Matyja,²⁸ W. Mitaroff,¹² H. Miyake,³² H. Miyata,³⁰ T. Mori,⁴
A. Murakami,³⁷ T. Nagamine,⁴⁵ Y. Nagasaka,¹⁰ T. Nakadaira,⁴⁶ E. Nakano,³¹ M. Nakao,⁹ H. Nakazawa,⁹
J. W. Nam,⁴⁰ Z. Natkaniec,²⁸ S. Nishida,¹⁷ O. Nitoh,⁴⁹ T. Nozaki,⁹ S. Ogawa,⁴³ T. Ohshima,²³ T. Okabe,²³
S. Okuno,¹⁵ S. L. Olsen,⁸ W. Ostrowicz,²⁸ H. Ozaki,⁹ P. Pakhlov,¹³ H. Palka,²⁸ C. W. Park,¹⁶ H. Park,¹⁸
K. S. Park,⁴⁰ L. S. Peak,⁴¹ J.-P. Perroud,¹⁹ L. E. Piilonen,⁵³ N. Root,² H. Sagawa,⁹ S. Saitoh,⁹ Y. Sakai,⁹
M. Satapathy,⁵² A. Satpathy,^{9,5} O. Schneider,¹⁹ A. J. Schwartz,⁵ T. Seki,⁴⁸ S. Semenov,¹³ K. Senyo,²³
M. E. Sevier,²² T. Shibata,³⁰ J. B. Singh,³³ N. Soni,³³ S. Stanič,^{9,*} M. Starič,¹⁴ A. Sugi,²³ K. Sumisawa,⁹
T. Sumiyoshi,⁴⁸ S. Suzuki,⁵⁴ S. K. Swain,⁸ T. Takahashi,³¹ F. Takasaki,⁹ J. Tanaka,⁴⁶ M. Tanaka,⁹ G. N. Taylor,²²
Y. Teramoto,³¹ T. Tomura,⁴⁶ K. Trabelsi,⁸ T. Tsuboyama,⁹ T. Tsukamoto,⁹ S. Uehara,⁹ K. Ueno,²⁷ S. Uno,⁹
G. Varner,⁸ K. E. Varvell,⁴¹ C. H. Wang,²⁶ J. G. Wang,⁵³ M.-Z. Wang,²⁷ M. Watanabe,³⁰ Y. Watanabe,⁴⁷
E. Won,¹⁶ B. D. Yabsley,⁵³ Y. Yamada,⁹ A. Yamaguchi,⁴⁵ H. Yamamoto,⁴⁵ Y. Yamashita,²⁹ M. Yamauchi,⁹
H. Yanai,³⁰ Heyoung Yang,³⁹ C. C. Zhang,¹¹ J. Zhang,⁵¹ Z. P. Zhang,³⁸ Y. Zheng,⁸ D. Žontar,^{20,14} and D. Zürcher¹⁹

(The Belle Collaboration)

¹Aomori University, Aomori

²Budker Institute of Nuclear Physics, Novosibirsk

³Chiba University, Chiba

⁴Chuo University, Tokyo

⁵University of Cincinnati, Cincinnati, Ohio 45221

⁶University of Frankfurt, Frankfurt

⁷Gyeongsang National University, Chinju

⁸University of Hawaii, Honolulu, Hawaii 96822

⁹High Energy Accelerator Research Organization (KEK), Tsukuba

¹⁰Hiroshima Institute of Technology, Hiroshima

¹¹Institute of High Energy Physics, Chinese Academy of Sciences, Beijing

¹²Institute of High Energy Physics, Vienna

¹³Institute for Theoretical and Experimental Physics, Moscow

¹⁴J. Stefan Institute, Ljubljana

¹⁵Kanagawa University, Yokohama

¹⁶Korea University, Seoul

¹⁷Kyoto University, Kyoto

¹⁸Kyungpook National University, Taegu

¹⁹Institut de Physique des Hautes Énergies, Université de Lausanne, Lausanne

- ²⁰University of Ljubljana, Ljubljana
²¹University of Maribor, Maribor
²²University of Melbourne, Victoria
²³Nagoya University, Nagoya
²⁴Nara Women's University, Nara
²⁵National Kaohsiung Normal University, Kaohsiung
²⁶National Lien-Ho Institute of Technology, Miao Li
²⁷Department of Physics, National Taiwan University, Taipei
²⁸H. Niewodniczanski Institute of Nuclear Physics, Krakow
²⁹Nihon Dental College, Niigata
³⁰Niigata University, Niigata
³¹Osaka City University, Osaka
³²Osaka University, Osaka
³³Panjab University, Chandigarh
³⁴Peking University, Beijing
³⁵Princeton University, Princeton, New Jersey 08545
³⁶RIKEN BNL Research Center, Upton, New York 11973
³⁷Saga University, Saga
³⁸University of Science and Technology of China, Hefei
³⁹Seoul National University, Seoul
⁴⁰Sungkyunkwan University, Suwon
⁴¹University of Sydney, Sydney NSW
⁴²Tata Institute of Fundamental Research, Bombay
⁴³Toho University, Funabashi
⁴⁴Tohoku Gakuin University, Tagajo
⁴⁵Tohoku University, Sendai
⁴⁶Department of Physics, University of Tokyo, Tokyo
⁴⁷Tokyo Institute of Technology, Tokyo
⁴⁸Tokyo Metropolitan University, Tokyo
⁴⁹Tokyo University of Agriculture and Technology, Tokyo
⁵⁰Toyama National College of Maritime Technology, Toyama
⁵¹University of Tsukuba, Tsukuba
⁵²Utkal University, Bhubaneswer
⁵³Virginia Polytechnic Institute and State University, Blacksburg, Virginia 24061
⁵⁴Yokkaichi University, Yokkaichi
⁵⁵Yonsei University, Seoul

We report an improved measurement of the partial-rate CP asymmetry in $B^\pm \rightarrow \bar{K}^0 \pi^\pm$ decays. The analysis is based on a data sample of 85 million $B\bar{B}$ pairs collected at the $\Upsilon(4S)$ resonance with the Belle detector at the KEKB e^+e^- storage ring. We measure $\mathcal{A}_{CP}(\bar{K}^0 \pi^\pm) = 0.07^{+0.09}_{-0.08}{}^{+0.01}_{-0.03}$, where the first and second errors are statistical and systematic, respectively; the corresponding 90% confidence-level interval is $-0.10 < \mathcal{A}_{CP}(\bar{K}^0 \pi^\pm) < 0.22$.

PACS numbers: 11.30.Er, 12.15.Hh, 13.25.Hw, 14.40.Nd

In the Kobayashi-Maskawa (KM) model [1], CP violation arises from a complex phase in the quark-mixing matrix of the weak interaction. This idea is strongly supported by the observation of mixing-induced CP violation at the B -factories [2]. Direct CP violation (DCPV) is also expected in the KM scheme and has been observed in the K meson system [3]. However, DCPV has not yet been observed in the B meson system.

Charmless hadronic B decays can provide opportunities to observe DCPV [4, 5, 6, 7, 8]. Many of these decays include contributions from both $b \rightarrow u$ tree and $b \rightarrow s$ penguin diagrams and the interference between these two processes can produce a partial-rate CP asymmetry:

$$\begin{aligned} \mathcal{A}_{CP} &= \frac{\Gamma(\bar{B} \rightarrow \bar{f}) - \Gamma(B \rightarrow f)}{\Gamma(\bar{B} \rightarrow \bar{f}) + \Gamma(B \rightarrow f)} \\ &= \frac{2|A_T||A_P| \sin \delta \sin \phi}{|A_T|^2 + |A_P|^2 + 2|A_T||A_P| \cos \delta \cos \phi}. \end{aligned}$$

Here $\Gamma(B \rightarrow f)$ denotes the partial width of either a B_d^0 or B^+ meson decaying into a flavor-specific final state f and $\Gamma(\bar{B} \rightarrow \bar{f})$ represents that of the charge conjugate decay; A_T and A_P represent the tree and penguin amplitudes; and

δ and ϕ stand for the CP -conserving and CP -violating relative phases, respectively, between A_T and A_P . In order to have a sizable \mathcal{A}_{CP} , both phase differences have to be non-zero, i.e. $\delta \neq 0$ and $\phi \neq 0$, and the tree and penguin amplitudes should be of comparable size ($|A_T| \sim |A_P|$).

The decay $B^\pm \rightarrow \bar{K}^0 \pi^\pm$ is almost a pure $b \rightarrow s$ penguin process and, thus, no sizable asymmetry is expected in the context of the Standard Model (SM) [9, 10]. However, our previously published result, based on an analysis of a 29 fb^{-1} data sample, was $\mathcal{A}_{CP}(\bar{K}^0 \pi^\pm) = 0.46 \pm 0.15 \pm 0.02$ [6]. An asymmetry of this magnitude cannot be explained in the SM, even with the inclusion of interference of the basic penguin amplitude with a large $B^\pm \rightarrow (K^\pm \pi^0)_{\text{tree}} \rightarrow \bar{K}^0 \pi^\pm$ re-scattering process [11], and would be an indication of a new physics contribution in the penguin loop [12]. It is important to verify whether the central value persists with improved precision.

In this paper, we report an updated measurement of the partial-rate CP asymmetry in $B^\pm \rightarrow \bar{K}^0 \pi^\pm$ decays based on a 78 fb^{-1} data sample collected at the $\Upsilon(4S)$ resonance, corresponding to 85.0 ± 0.5 million $B\bar{B}$ pairs, with the Belle detector [13] at the KEKB e^+e^- storage ring [14]. This is approximately three times as much data as the sample that was used for the previous measurement and significantly improves the statistical precision. Throughout this paper, the partial-rate CP asymmetry $\mathcal{A}_{CP}(\bar{K}^0 \pi^\pm)$ is defined as

$$\mathcal{A}_{CP}(\bar{K}^0 \pi^\pm) \equiv \frac{N(K_S^0 \pi^-) - N(K_S^0 \pi^+)}{N(K_S^0 \pi^-) + N(K_S^0 \pi^+)},$$

where $N(K_S^0 \pi^-)$ denotes the yield of $B^- \rightarrow K_S^0 \pi^-$ decay and $N(K_S^0 \pi^+)$ represents that of the charge conjugate mode.

The Belle detector is a large-solid-angle spectrometer that consists of a three-layer silicon vertex detector (SVD), a 50-layer central drift chamber (CDC), an array of threshold Čerenkov counters with silica aerogel radiators (ACC), time-of-flight scintillation counters (TOF), and an electromagnetic calorimeter comprised of CsI(Tl) crystals (ECL) located inside a superconducting solenoid coil that provides a 1.5 T magnetic field. An iron flux-return located outside of the coil is instrumented to detect K_L^0 mesons and to identify muons (KLM). A detailed description of the Belle detector can be found elsewhere [13].

The analysis procedure is the same as described in Ref. [6]. Candidate B^\pm mesons are reconstructed using high momentum π^\pm and K_S^0 mesons. For candidate π^\pm mesons, charged tracks are required to originate from the interaction region based on their impact parameters.

In Belle, high momentum π^\pm and K^\pm mesons are distinguished by their associated Čerenkov light yield ($N_{\text{p.e.}}$) in the ACC and the ionization energy loss (dE/dx) in the CDC. These quantities are used to form a particle identification (PID) likelihood ratio $\mathcal{R}_\pi = \mathcal{L}_\pi / (\mathcal{L}_\pi + \mathcal{L}_K)$, where \mathcal{L}_π denotes the product of the individual likelihoods of $N_{\text{p.e.}}$ and dE/dx for π^\pm mesons; \mathcal{L}_K is the product for K^\pm mesons. For the \mathcal{R}_π requirement used in this analysis, π^\pm mesons are identified with an efficiency of 91% and there is a 10% K^\pm misidentification rate. The efficiency and fake rate are estimated by comparing the \bar{D}^0 yields in a sample of $D^{*\pm}$ -tagged $\bar{D}^0 \rightarrow K^\mp \pi^\pm$ decays before and after the application of the high momentum PID requirements. A similar likelihood ratio that also includes the energy deposit in the ECL is used to identify electrons; positively identified electrons are rejected. Candidate K_S^0 mesons are reconstructed using pairs of oppositely charged tracks that have an invariant mass ($m_{\pi\pi}$) in the range $480 < m_{\pi\pi} < 516 \text{ MeV}/c^2$. A candidate must have a displaced vertex and flight direction consistent with a K_S^0 originating from the IP.

Signal candidates are identified using the beam-energy constrained mass $m_{bc} = \sqrt{E_{\text{beam}}^2 - p_B^{*2}}$ and the energy difference $\Delta E = E_B^* - E_{\text{beam}}$, where $E_{\text{beam}} = 5.29 \text{ GeV}$ and p_B^* and E_B^* are the momentum and energy of the reconstructed B meson in the e^+e^- center-of-mass frame.

The dominant background comes from the $e^+e^- \rightarrow q\bar{q}$ ($q = u, d, s, c$) continuum process; backgrounds from $b \rightarrow c$ decays are negligible because the momenta of the decay products are smaller than those of the signal K_S^0 and π^\pm . We discriminate the signal from the $q\bar{q}$ background by the event topology. This is quantified by the Super-Fox-Wolfram (SFW) variable [6, 15], which is formed from modified Fox-Wolfram moments that are combined using a Fisher discriminant [16] into a single variable. The angle of the B -meson's flight direction with respect to the beam axis (θ_B) provides additional discrimination. A likelihood ratio $\mathcal{R}_s = \mathcal{L}_s / (\mathcal{L}_s + \mathcal{L}_{q\bar{q}})$ is calculated, where \mathcal{L}_s ($\mathcal{L}_{q\bar{q}}$) denotes the product of the individual SFW and θ_B likelihoods for signal ($q\bar{q}$ background). The probability density functions (PDFs) are derived from GEANT-based Monte Carlo (MC) simulations [17] for the signal and m_{bc} sideband ($5.2 < m_{bc} < 5.26 \text{ GeV}/c^2$) data for the $q\bar{q}$ background. We make a requirement on \mathcal{R}_s that eliminates 88% of the $q\bar{q}$ background while retaining 73% of the signal.

Signal yields are extracted from the ΔE distributions of events in the m_{bc} signal region ($5.271 < m_{bc} < 5.287 \text{ GeV}/c^2$), separately for the $K_S^0 \pi^+$ and $K_S^0 \pi^-$ final states. The signal reconstruction efficiency [18] is estimated to be 12% based on the MC. The ΔE distributions are fitted using a binned maximum likelihood fit with three components: the signal, $q\bar{q}$ background, and other charmless B decays, as shown in Fig. 1. The signal PDF

is modeled with a Gaussian distribution taken from the signal MC and calibrated using a $B^\pm \rightarrow \overline{D}^0(\rightarrow K^\pm\pi^\mp)\pi^\pm$ sample where a similar reconstruction procedure is applied. For the $q\bar{q}$ background, the PDF is modeled with a second-order polynomial with a shape that is determined from the m_{bc} sideband data. For other charmless B decays, the PDF is taken from a smoothed histogram of a large MC sample. (The enhancement in the lower ΔE region is due to charmless B decay modes with an additional π meson.) Except for the signal peak positions, the same PDF shape parameters are used for both B^+ and B^- samples. The signal peak positions are determined separately for the B^+ and B^- samples since a small systematic difference between the two samples is observed. (This is discussed below.) In the fit procedure, all of the PDF shape parameters are fixed and all the normalizations are free parameters. The signal yields are found to be $N(K_S^0\pi^+) = 104.4^{+13.2}_{-12.5}$ and $N(K_S^0\pi^-) = 119.1^{+13.8}_{-13.1}$, and the partial-rate CP asymmetry is determined to be $\mathcal{A}_{CP}(\overline{K}^0\pi^\pm) = 0.07^{+0.09}_{-0.08}$.

The stability of $\mathcal{A}_{CP}(\overline{K}^0\pi^\pm)$ as a function of the the selection requirements is tested by varying the $q\bar{q}$ suppression requirement. As shown in Fig. 2, the value of $\mathcal{A}_{CP}(\overline{K}^0\pi^\pm)$ is stable when this requirement is changed.

Detector-based biases in $K_S^0\pi^\pm$ reconstruction are investigated using a sample of inclusive, high momentum continuum $D^\pm \rightarrow K_S^0\pi^\pm$ decays, where the daughter particles are required to satisfy the same kinematic requirements and reconstruction criteria as used for the signal. Separate fits to the D^\pm mass distributions, shown in Fig. 3, indicate that the signal mass resolutions for the B^+ and B^- samples are consistent, but there is a 1.0 ± 0.1 MeV/ c^2 difference in the mass peak positions. This difference in the peak positions is caused by a difference between the momentum measurement for high momentum negative and positive tracks that is attributed to a residual detector misalignment. After accounting for this difference in peak positions, $\mathcal{A}_{CP}(D^\pm \rightarrow K_S^0\pi^\pm)$ is determined and listed in Table I. Here the sign convention in the definition of $\mathcal{A}_{CP}(D^\pm \rightarrow K_S^0\pi^\pm)$ follows that of $\mathcal{A}_{CP}(\overline{K}^0\pi^\pm)$. The observed $(2.0 \pm 0.8)\%$ asymmetry is treated as a possible bias, and -2.8% is assigned as a systematic error in the $\mathcal{A}_{CP}(\overline{K}^0\pi^\pm)$ measurement.

Possible biases in the B reconstruction are examined using a sample of $B^\pm \rightarrow \overline{D}^0(\rightarrow K^\pm\pi^\mp)\pi^\pm$ decays where the entire reconstruction procedure, except for the K_S^0 reconstruction, is applied. Fits to the separate B^+ and B^- ΔE distributions, shown in Fig. 4, confirm that the resolutions are consistent between the two samples, while a 3.2 ± 0.5 MeV difference in peak positions, due to the same effect that was found in the $D^\pm \rightarrow K_S^0\pi^\pm$ sample, is observed. After accounting for the difference in ΔE peak positions, $\mathcal{A}_{CP}(B^\pm \rightarrow \overline{D}^0\pi^\pm)$ is determined and listed in Table I. The absence of an asymmetry indicates there is no bias. Biases in the high momentum PID and $q\bar{q}$ suppression are also examined by removing each of them in the $\mathcal{A}_{CP}(B^\pm \rightarrow \overline{D}^0\pi^\pm)$ measurement. The results are given in Table I. No biases are observed.

Possible asymmetries in the detector response and reconstruction for the $q\bar{q}$ background are checked using events in the m_{bc} sideband region. The application of the entire reconstruction procedure confirms that the ΔE shapes of the B^+ and B^- samples are consistent, and no bias is observed, as indicated in Table I. The absence of \mathcal{R}_π - and \mathcal{R}_s -related biases are confirmed in the same manner as for the $B^\pm \rightarrow \overline{D}^0(\rightarrow K^\pm\pi^\mp)\pi^\pm$ sample.

In order to study the sensitivity to the signal and $q\bar{q}$ background PDF shapes, each shape parameter is independently varied by its 1σ error. In addition, the signal shape parameters are also estimated from the actual $B^\pm \rightarrow K_S^0\pi^\pm$ samples by allowing them to be free parameters in the fits. The uncertainty in the contribution from other charmless B decays is estimated from the change in the asymmetry by fitting the region of $\Delta E > -0.1$ GeV without those decays. The resulting relative changes in asymmetries are added in quadrature giving the fitting systematics of $+0.014$ and -0.006 .

Because of the difference between the results presented here and the sizable asymmetry in our previous measurement, the asymmetries of different data sub-samples are examined. Figure 5 shows $\mathcal{A}_{CP}(\overline{K}^0\pi^\pm)$ for each data sub-sample together with $\mathcal{A}_{CP}(D^\pm \rightarrow K_S^0\pi^\pm)$ as a reference. The variation of $\mathcal{A}_{CP}(\overline{K}^0\pi^\pm)$ is independent of that in $\mathcal{A}_{CP}(D^\pm \rightarrow K_S^0\pi^\pm)$ and is consistent with statistical fluctuations.

The total systematic error in the $\mathcal{A}_{CP}(\overline{K}^0\pi^\pm)$ is evaluated from the quadratic sum of the $K_S^0\pi^\pm$ reconstruction bias and ΔE fitting systematics. Finally, the asymmetry

$$\mathcal{A}_{CP}(\overline{K}^0\pi^\pm) = 0.07^{+0.09}_{-0.08}{}^{+0.01}_{-0.03}$$

is obtained and a 90% confidence level interval

$$-0.10 < \mathcal{A}_{CP}(\overline{K}^0\pi^\pm) < 0.22,$$

is set, where Gaussian statistics are assumed and the systematic error is added linearly.

In conclusion, we have measured the partial-rate CP asymmetry in $B^\pm \rightarrow \bar{K}^0 \pi^\pm$ with 85 million $B\bar{B}$ pairs collected on the $\Upsilon(4S)$ resonance at the Belle experiment. The resulting $\mathcal{A}_{CP}(\bar{K}^0 \pi^\pm) = 0.07^{+0.09}_{-0.08}{}^{+0.01}_{-0.03}$ is consistent with zero at the current level of statistical precision. The 90% confidence level interval $-0.10 < \mathcal{A}_{CP}(\bar{K}^0 \pi^\pm) < 0.22$ is set, which is consistent with other measurements [7, 8]. This result has a statistical precision below 10% and supersedes our previous measurement [6]. We do not observe a significant partial-rate CP asymmetry in $B^\pm \rightarrow \bar{K}^0 \pi^\pm$ and attribute the sizable $\mathcal{A}_{CP}(\bar{K}^0 \pi^\pm)$ found previously in a much smaller data sample to a statistical fluctuation.

We are grateful to Y. Okada for useful discussions and comments. We wish to thank the KEKB accelerator group for the excellent operation of the KEKB accelerator. We acknowledge support from the Ministry of Education, Culture, Sports, Science, and Technology of Japan and the Japan Society for the Promotion of Science; the Australian Research Council and the Australian Department of Industry, Science and Resources; the National Science Foundation of China under contract No. 10175071; the Department of Science and Technology of India; the BK21 program of the Ministry of Education of Korea and the CHEP SRC program of the Korea Science and Engineering Foundation; the Polish State Committee for Scientific Research under contract No. 2P03B 17017; the Ministry of Science and Technology of the Russian Federation; the Ministry of Education, Science and Sport of the Republic of Slovenia; the National Science Council and the Ministry of Education of Taiwan; and the U.S. Department of Energy.

* on leave from Nova Gorica Polytechnic, Nova Gorica

- [1] M. Kobayashi and T. Maskawa, Prog. Theor. Phys. **49**, 652 (1973).
- [2] Belle Collaboration, K. Abe *et al.*, Phys. Rev. Lett. **87**, 091802 (2001); Phys. Rev. **D66**, 071102(R) (2002); BABAR Collaboration, B. Aubert *et al.*, Phys. Rev. Lett. **87**, 091801 (2001); **89**, 201802 (2002).
- [3] KTeV Collaboration, A. Alavi-Harati *et al.*, Phys. Rev. Lett. **83**, 22 (1999); NA48 Collaboration, J.R. Batley *et al.*, Phys. Lett. **B544**, 97 (2002).
- [4] See for a recent review R. Fleischer, hep-ph/0210323 (2002).
- [5] Belle Collaboration, K. Abe *et al.*, Phys. Rev. **D64**, 071101(R) (2001); Phys. Rev. Lett. **89**, 071801 (2002); hep-ex/0301032 (2003).
- [6] Belle Collaboration, B.C.K. Casey *et al.*, Phys. Rev. **D66**, 092002 (2002).
- [7] CLEO Collaboration, S. Chen *et al.*, Phys. Rev. Lett. **85**, 525 (2000).
- [8] BABAR Collaboration, B. Aubert *et al.*, Phys. Rev. Lett. **87**, 151802 (2001); Phys. Rev. **D65**, 051502(R) (2001); Phys. Rev. Lett. **89**, 281802 (2002); hep-ex/0303028 (2003).
- [9] See, for example, M. Beneke *et al.*, Nucl. Phys. **B606**, 245 (2001).
- [10] See, for example, A.I. Sanda and K. Ukai, Prog. Theor. Phys. **107**, 421 (2002); Y.-Y. Keum and A.I. Sanda, hep-ph/0209014 (2002).
- [11] See, for example, A.J. Buras, R. Fleischer and T. Mannel, Nucl. Phys. **B533**, 3 (1998); W.S. Hou and K.C. Yang, Phys. Rev. Lett. **84**, 4806 (2000).
- [12] See, for example, X.G. He, W.S. Hou and K.C. Yang, Phys. Rev. Lett. **81**, 5738 (1998); R. Fleischer and T. Mannel, hep-ph/9706261 (1997).
- [13] Belle Collaboration, A. Abashian *et al.*, Nucl. Inst. Meth. **A479**, 117 (2002).
- [14] E. Kikutani (ed.), Nucl. Inst. Meth. **A499**, 1 (2003).
- [15] G. Fox and S. Wolfram, Phys. Rev. Lett. **41**, 1581 (1978).
- [16] R.A. Fisher, Annals of Eugenics **7**, 179 (1936).
- [17] R. Brun *et al.*, GEANT 3.21, CERN Report No. DD/EE/84-1 (1987).
- [18] The signal reconstruction efficiency includes branching fractions of $K^0 \rightarrow K_S^0$ and $K_S^0 \rightarrow \pi^+ \pi^-$.

TABLE I: Summary of the detector-based bias tests. For tests other than those with the $D^\pm \rightarrow K_S^0 \pi^\pm$ sample, \mathcal{A}_{CP} values determined without the high momentum PID (\mathcal{R}_π) and $q\bar{q}$ suppression (\mathcal{R}_s) requirements are also listed.

Samples		\mathcal{A}_{CP} [%]
$D^\pm \rightarrow K_S^0 \pi^\pm$		2.0 ± 0.8
$B^\pm \rightarrow \bar{D}^0(\rightarrow K^\pm \pi^\mp) \pi^\pm$		0.6 ± 1.7
	w/o \mathcal{R}_π	0.0 ± 1.5
	w/o \mathcal{R}_s	0.0 ± 1.4
$B^\pm \rightarrow K_S^0 \pi^\pm$ m_{bc} sideband data		0.9 ± 1.3
	w/o \mathcal{R}_π	0.5 ± 0.9
	w/o \mathcal{R}_s	0.5 ± 0.4

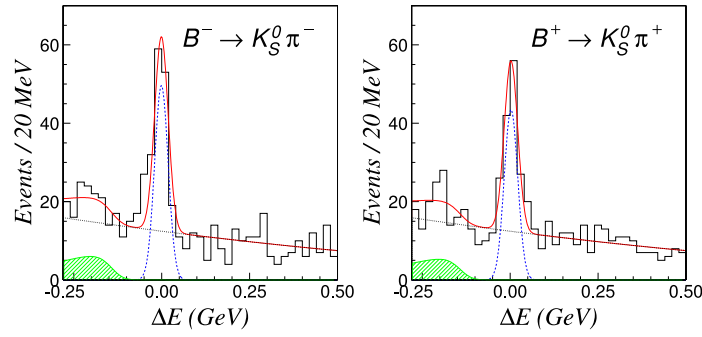


FIG. 1: The ΔE distributions for the $B^\pm \rightarrow K_S^0 \pi^\pm$ candidates divided into B^- (left) and B^+ (right) samples. The fit results are shown as the solid, dashed and dotted curves for the total, signal and $q\bar{q}$ background, respectively; the hatched area indicates the contribution from other charmless B decays.

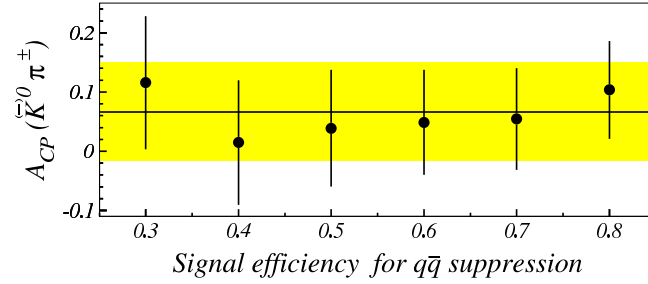


FIG. 2: $\mathcal{A}_{CP}(K_S^0 \pi^\pm)$ as a function of the signal efficiency of the $q\bar{q}$ suppression (\mathcal{R}_s) selection. The horizontal line and hatched area indicate the $\mathcal{A}_{CP}(K_S^0 \pi^\pm)$ value and its statistical error for the \mathcal{R}_s requirement used in the actual measurement. Note that the statistical errors for the different data points are strongly correlated.

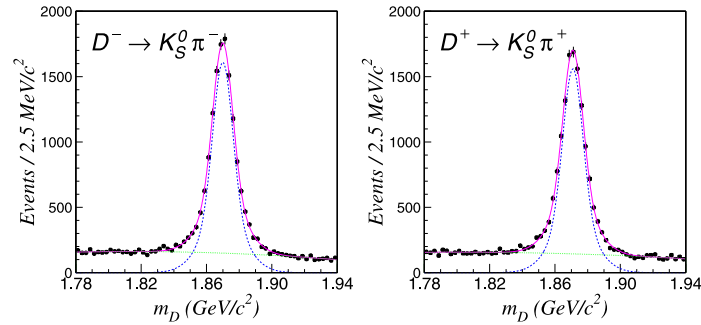


FIG. 3: The mass spectra for the $D^\pm \rightarrow K_S^0 \pi^\pm$ candidates separated into D^- (left) and D^+ (right) samples, where the kinematic requirements and daughter particle reconstruction are the same as used for the $B^\pm \rightarrow K_S^0 \pi^\pm$ signal. The fit results are shown as the solid, dashed and dotted curves for the total, $D^\pm \rightarrow K_S^0 \pi^\pm$ and combinatorial background, respectively.

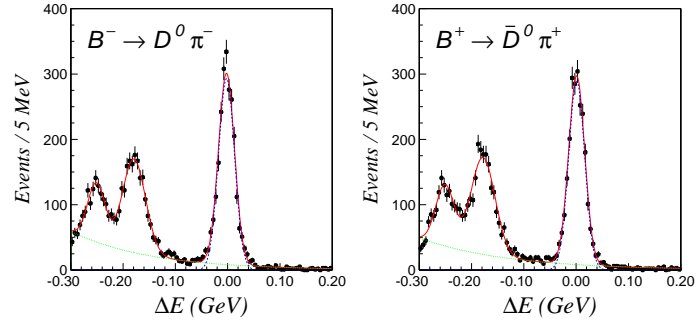


FIG. 4: The ΔE distributions for $B^\pm \rightarrow \bar{D}^0(\rightarrow K^\pm \pi^\mp) \pi^\pm$ candidates separately for the B^- (left) and B^+ (right) samples after application of the entire reconstruction procedure other than that for the K_S^0 . The fit results are shown as the solid, dashed and dotted curves for the total, $B^\pm \rightarrow \bar{D}^0(\rightarrow K^\pm \pi^\mp) \pi^\pm$ and combinatorial background, respectively. The enhancement in the lower ΔE region contains backgrounds from $B \rightarrow D^* \pi^\pm$ and $D^0 \rho$.

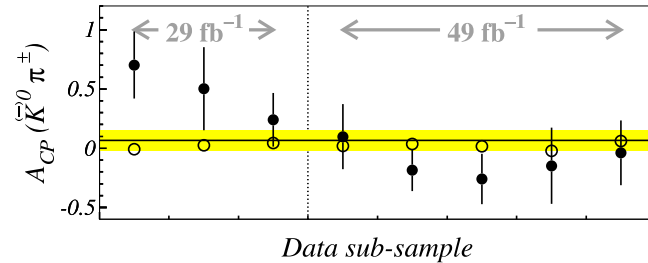


FIG. 5: $\mathcal{A}_{CP}(\bar{K}^0 \pi^\pm)$ in each data sub-sample. The horizontal line and hatched area show the central value and the 1σ statistical error of the $\mathcal{A}_{CP}(\bar{K}^0 \pi^\pm)$ result reported here. The solid points with the statistical error bars represent the $\mathcal{A}_{CP}(\bar{K}^0 \pi^\pm)$ result obtained for each data sub-sample; the open points show $\mathcal{A}_{CP}(D^\pm \rightarrow K_S^0 \pi^\pm)$. The sum of the three left-most points corresponds to the 29 fb^{-1} data sample used in our previous measurement.